

High field properties of geometrically frustrated magnets

M. E. ZHITOMIRSKY¹ and Hirokazu TSUNETSUGU²

¹*Commissariat à l'Energie Atomique, DSM/DRFMC/SPSMS,
38054 Grenoble, France,*

²*Yukawa Institute for Theoretical Physics, Kyoto University,
Kyoto 606-8502, Japan*

(Received June 14, 2005)

Above the saturation field, geometrically frustrated quantum antiferromagnets have dispersionless low-energy branches of excitations corresponding to localized spin-flip modes. Transition into a partially magnetized state occurs via condensation of an infinite number of degrees of freedom. The ground state below the phase transition is a magnon crystal, which breaks only translational symmetry and preserves spin-rotations about the field direction. We give a detailed review of recent works on physics of such phase transitions and present further theoretical developments. Specifically, the low-energy degrees of freedom of a spin-1/2 kagomé antiferromagnet are mapped to a hard hexagon gas on a triangular lattice. Such a mapping allows to obtain a quantitative description of the magnetothermodynamics of a quantum kagomé antiferromagnet from the exact solution for a hard hexagon gas. In particular, we find the exact critical behavior at the transition into a magnon crystal state, the universal value of the entropy at the saturation field, and the position of peaks in temperature- and field-dependence of the specific heat. Analogous mapping is presented for the sawtooth chain, which is mapped onto a model of classical hard dimers on a chain. The finite macroscopic entropies of geometrically frustrated magnets at the saturation field lead to a large magnetocaloric effect.

§1. Introduction

Theoretical investigation of finite field properties of geometrically frustrated magnets is a new rapidly developing direction of research, which is to a large extent stimulated by the experimental studies. There are now a few examples of frustrated magnetic compounds such as pyrochlore $\text{Gd}_2\text{Ti}_2\text{O}_7$,¹⁾ garnet $\text{Gd}_3\text{Ga}_5\text{O}_{12}$,²⁾ and spinel CdCr_2O_4 ,³⁾ for which full or partial reconstruction of the phase diagram in magnetic field has been done. From theoretical point of view, an applied magnetic field competes with antiparallel alignment of spins favored by antiferromagnetic exchange interaction and creates an extra source of frustration. This may lead to various interesting phenomena at high magnetic fields such as exotic quantum ground states, novel types of the critical behavior, the magnetization jumps and plateaus and so on. Here we give a detailed overview and present further development of the recent theoretical works on a universal behavior of geometrically frustrated magnets in the vicinity of the saturation field H_s .⁴⁾⁻¹⁰⁾

At high fields Heisenberg antiferromagnets exhibit a phase transition between a fully polarized state and a state with reduced magnetization. A partially magnetized state typically breaks spin-rotational symmetry about the field direction and has a long-range order of transverse spin components. Since the quantum ground

state at $H > H_s$ is known exactly one can also calculate an exact spectrum of single magnon excitations $\omega(\mathbf{k})$.¹¹⁾ For ordinary nonfrustrated antiferromagnets $\omega(\mathbf{k})$ has a well defined minimum at a certain wave-vector \mathbf{Q} with a gap $\Delta = H - H_s$. The high-field transition can be described as a Bose condensation of spin-flips with momenta $\mathbf{k} = \mathbf{Q}$.¹²⁾ The above simple picture fails, however, for frustrated magnets. Reflecting degeneracy of classical ground states at $H < H_s$, the magnon dispersion at $H > H_s$ has a continuous set of degenerate minima. For two well-known frustrated models, Heisenberg antiferromagnets on a face centered cubic lattice and on a frustrated square lattice, single magnon spectra in the saturated phase are degenerate on lines in the Brillouin zone. The phase transition at $H = H_s$ is, therefore, associated with condensation of an infinite number of soft modes. This yields an effective dimensionality reduction and change in the critical behavior.¹³⁾ Geometrically frustrated antiferromagnets on kagomé, checkerboard, and pyrochlore lattices exhibit even stronger degeneracy with a completely flat lowest branch of magnons: $\omega(\mathbf{k}) \equiv H - H_s$. The theory of such phase transitions is discussed below on two examples of the sawtooth chain and the kagomé antiferromagnet, Fig. 1.

§2. Localized magnons

We consider nearest-neighbor Heisenberg antiferromagnets in an external field

$$\hat{\mathcal{H}} = \sum_{\langle ij \rangle} J_{ij} \mathbf{S}_i \cdot \mathbf{S}_j - \mathbf{H} \cdot \sum_i \mathbf{S}_i \quad (2.1)$$

with a general value S of on-site spins. The exchange coupling constants J_{ij} connect only the nearest neighbor sites. The couplings are all the same for a kagomé lattice $J_{ij} \equiv J$, while the sawtooth chain is described by two exchange constants: J_1 for base-vertex bonds and J_2 for base-base bonds, see Fig. 1. Above the saturation field H_s the ground state of (2.1) is a ferromagnetic vacuum $|0\rangle = |\uparrow\uparrow\uparrow \dots\rangle$, where all spins are in a state with the maximum possible value of $S_i^z = S$. The low-lying excitations are spin flips $|i\rangle = S_i^- |0\rangle$. Diagonalizing the Heisenberg Hamiltonian (2.1) within one-magnon subspace, which is possible since $S_{\text{tot}}^z = \sum_i S_i^z$ commutes with $\hat{\mathcal{H}}$, one finds an exact one-particle spectrum.¹¹⁾

The primitive unit cell of a kagomé lattice contains three sites. Accordingly, there exist three branches of magnons for every wave-vector:

$$\omega_1(\mathbf{k}) = H - 6JS, \quad \omega_{2,3}(\mathbf{k}) = H - 3JS \pm JS\sqrt{3(1 + 2\gamma_{\mathbf{k}})}, \quad (2.2)$$

where $\gamma_{\mathbf{k}} = 1/6 \sum_l e^{i\mathbf{k}\cdot\mathbf{a}_l}$ is a sum over six nearest-neighbor sites on a triangular Bravais lattice. The lowest energy branch $\omega_1(\mathbf{k})$ has no dispersion and its energy vanishes at the saturation field $H_s = 6JS$. Among the two dispersive branches the lower one $\omega_3(\mathbf{k})$ has also a vanishing gap at the saturation field.

In the case of the sawtooth chain, one, generally, finds two dispersive branches of one-magnon excitations:

$$\omega_{1,2}(k) = H - 2J_1S - J_2S(1 - \cos k) \pm S\sqrt{J_2^2(1 - \cos k)^2 + 2J_1^2(1 + \cos k)}. \quad (2.3)$$

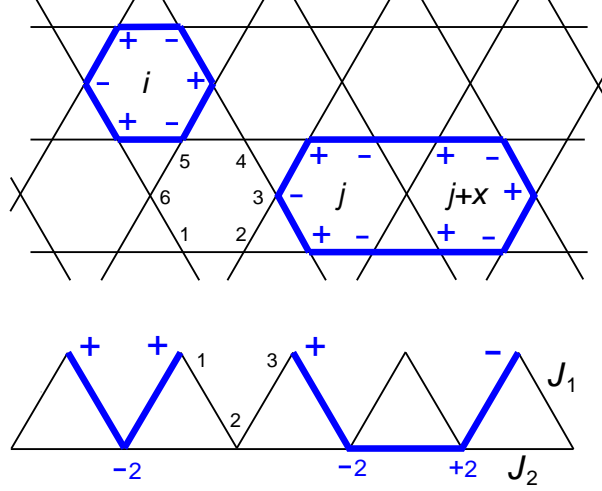


Fig. 1. Kagomé lattice (top) and the sawtooth chain (bottom) with localized magnons shown by thick lines. Amplitudes and phases of spin-down states are indicated near each site.

However, for a special choice of the coupling constants $J_2 = 0.5J_1$ ($J_1 \equiv J$), the lower branch becomes dispersionless:

$$\omega_1(k) = H - 4JS, \quad \omega_2(k) = H - JS(1 - \cos k). \quad (2.4)$$

The above two branches are separated by a finite gap $\Delta\omega = 2JS$.

The two formulated spin models are related to several magnetic materials. A kagomé lattice model is applicable, for example, for $\text{SrCr}_{9p}\text{Ga}_{12-9p}\text{O}_{19}$,¹⁴⁾ while the sawtooth chain describes magnetic delafossite $\text{YCuO}_{2.5}$.¹⁵⁾ Unfortunately, both compounds have rather large exchange constants $J \sim 500K$, which makes impossible to reach their high-field regimes $H \sim H_s$.

The dispersionless excitations correspond in real space to localized states. Spin flips are completely localized excitations in Ising models, while for Heisenberg interaction they hop between adjacent lattice sites and generally acquire a finite dispersion. In the two considered examples localization of spin flips is determined by lattice topology. For a kagomé lattice a simplest localized state corresponds to a magnon trapped on a hexagon void. Its wave function is given by

$$|\varphi_i\rangle = \frac{1}{\sqrt{12S}} \sum_{n=1}^6 (-1)^{n-1} S_{ni}^- |0\rangle, \quad (2.5)$$

where numbering of sites inside the i^{th} hexagon goes counterclockwise starting with the lower left corner, see Fig. 1. An outside spin on one of the triangles surrounding hexagon is connected to two sites, where a localized magnon has equal amplitudes and opposite phases. This produces destructive interference and the amplitude of spin flip on surrounding sites vanishes. The energy of the localized magnon (2.5) is $H - 6JS$, that is the same as $\omega_1(\mathbf{k})$. More complicated eigenstates with the same energy are constructed by taking closed loops with even number of spins, which

contain only two sites of any crossed triangle. The wave-function of a localized state has equal amplitudes on all chosen sites with alternating phases 0 and π . An example of a spin flip localized on two hexagons is shown in Fig. 1. The wave-function of such a state is a linear combination of simple hexagon states: $|\varphi_{j,j+x}\rangle \propto (|\varphi_j\rangle + |\varphi_{j+x}\rangle)$.

The localized modes on smallest hexagons can be used as a nonorthogonal basis in the subspace of one-magnon states from the dispersionless branch (2.2). To show this we note, first, that there are as many hexagons $N_h = N/3$ on an N -site lattice as the number of states in the Brillouin zone. Second, there is only one linear relation $\sum_i a_i |\varphi_i\rangle = 0$ between hexagon states for a cluster with periodic boundary conditions. It is constructed using the following arguments. An arbitrary site is shared between only two hexagons i and j . Wave-functions of the corresponding localized states have opposite signs for spin-flip amplitudes on the chosen site. Accordingly, the two amplitudes a_i and a_j from a linear relation must be equal. This property, when extended by induction, leads to a unique linear relation between hexagon states: a sum of all states with equal amplitudes $a_i = \text{const}$. The torus topology of a periodic cluster allows presence of a few other one-magnon states with the same energy $H - 6JS$, which cannot be decomposed into a hexagon basis. Such localized magnon states correspond to closed lines with nontrivial winding around the cluster. The localized magnon loops obtained as linear combinations of hexagon states have, in contrast, zero winding and are contractable into a point. In the thermodynamic limit $N \rightarrow \infty$ presence of a few states with nontrivial winding is unimportant and the localized hexagon states can be used as a real-space basis for the lowest branch in Eq. (2.2).

For the sawtooth chain a localized magnon is trapped in a valley between two triangles. Its wave-function is

$$|\varphi_i\rangle = \frac{1}{\sqrt{12S}}(S_{1i}^- - 2S_{2i}^- + S_{3i}^-)|0\rangle. \quad (2.6)$$

The numbering of spins inside one valley is shown in Fig. 1 with identity $\mathbf{S}_{1i} \equiv \mathbf{S}_{3,i-1}$. The probability for a spin-flip to jump to an outside site vanishes in the state (2.6) due to the relation $J_1 = 2J_2$. The $N/2$ valley states again form a complete nonorthogonal basis in the subspace of the lowest branch $\omega_1(k)$ (2.4). Since bottom (base) spins are not shared between adjacent valleys, the linear independence of states (2.6) is fulfilled even for finite periodic chains. A more extended localized state on a sawtooth chain shown in Fig. 1 is a linear combination of states in the two adjacent valleys.

Localized one-magnon states allow to construct a class of exact multiparticle states. Configurations, where localized spin flips occupy isolated clusters, become exact multimagnon states of the quantum spin Hamiltonian. Note, that for nonfrustrated quantum magnets in two or three dimensions, it is not possible to construct exact multiparticle states beyond the two-magnon subsector.¹¹⁾ Among all exact eigenstates with noninteracting localized magnons, states with the highest density of spin flips play a special role. These are constructed as close-packed structures of magnons localized on smallest clusters: hexagons or valleys. For a kagomé lattice the close-packed structure is constructed by putting localized magnons on every third hexagon, see Fig. 2. Such a magnon crystal with $N_{\text{max}} = N/9$ localized spin-flips

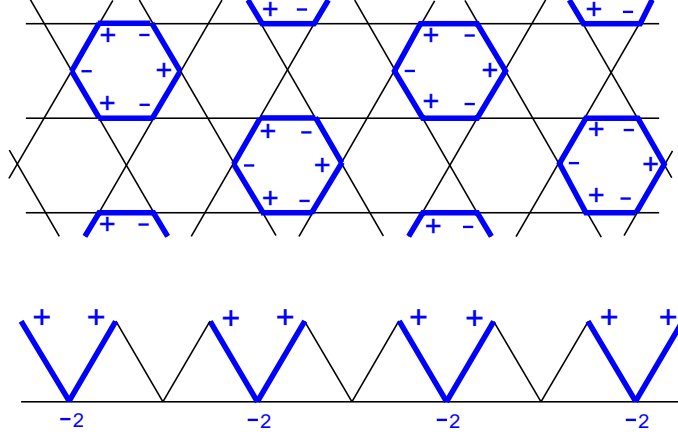


Fig. 2. Magnon crystals built from localized spin flips for a kagomé lattice (top) and the sawtooth chain (bottom).

breaks a three-fold translational symmetry of the magnetic Hamiltonian. Transverse components of spin operators on sites belonging to different localized magnons remain uncorrelated. The magnon crystal does not break, therefore, spin-rotational symmetry about z -axis. A magnon crystal for the sawtooth chain has $N_{\max} = N/4$ localized spin-flips and is two-fold degenerate.

Since isolated localized magnons do not interact with each other, it is plausible that they correspond to the lowest energy states in every n -magnon subsector with $n \leq N_{\max}$. The proof of the above property is easily formulated for lattices with a uniform exchange constant $J_{ij} = J$ like kagomé, checkerboard, and pyrochlore antiferromagnets.⁵⁾⁻⁷⁾ Let us consider, for simplicity, only $S = 1/2$ case. The Heisenberg Hamiltonian (2.1) can be split into an Ising and a transverse parts according to

$$\hat{\mathcal{H}}^{zz} = J \sum_{\langle ij \rangle} S_i^z S_j^z - H \sum_i S_i^z, \quad \hat{\mathcal{H}}^\perp = \frac{1}{2} J \sum_{\langle ij \rangle} (S_i^+ S_j^- + S_i^- S_j^+). \quad (2.7)$$

Below we always subtract energy of the ferromagnetic state from $\hat{\mathcal{H}}^{zz}$. A quantum state of n isolated localized magnons is an eigenstate of $\hat{\mathcal{H}}$ with $E_n = n(H - H_s)$, where $H_s = 3J$ for a spin-1/2 antiferromagnet on a kagomé lattice. In addition, such a state is also an eigenstate of $\hat{\mathcal{H}}^{zz}$ and $\hat{\mathcal{H}}^\perp$ with $E_n^{zz} = n(H - 2J)$ and $E_n^\perp = -nJ$, respectively. The idea of the proof is to show that for an arbitrary n -magnon state: $\langle \hat{\mathcal{H}}^{zz} \rangle \geq E_n^{zz}$ and $\langle \hat{\mathcal{H}}^\perp \rangle \geq E_n^\perp$.

For $\hat{\mathcal{H}}^{zz}$ the formulated relation holds trivially: once all spin flips occupy different bonds the Ising part of the Hamiltonian has the minimal energy: $E_n^{zz} = n(H - \frac{1}{2}zJ)$, where $z = 4$ is the number of nearest neighbors for a kagomé lattice. In order to show that a similar inequality holds for the transverse part $\hat{\mathcal{H}}^\perp$ we map the n -magnon subspace of a spin-1/2 model onto the Hilbert space of n hard-core bosons \mathcal{B}_n . The transverse part of the Heisenberg Hamiltonian is, then, the kinetic energy of bosons $\hat{\mathcal{H}}^\perp \equiv \hat{\mathcal{K}}$. In addition, we define the Hilbert space of n bosons without the hard-core constraint \mathcal{B}_{n0} with an evident relation $\mathcal{B}_n \subset \mathcal{B}_{n0}$. The minimum of the kinetic

energy is easily found in \mathcal{B}_{n0} : all n particles must occupy one of the lowest energy single-particle states with the kinetic energy $E_{\mathcal{K}} = -J$ found from Eq. (2.2). If the hard-core constraint is imposed, then, from the variational principle, the expectation value of $\hat{\mathcal{K}}$ can only increase: $\min\langle\hat{\mathcal{K}}\rangle_{\mathcal{B}_n} \geq \min\langle\hat{\mathcal{K}}\rangle_{\mathcal{B}_{n0}} = -nJ = E_n^\perp$.

The above proof does not immediately apply to the sawtooth chain, which has nonequivalent bonds. A localized magnon (2.6) is an eigenstate of the total Hamiltonian $\hat{\mathcal{H}}$, but not of $\hat{\mathcal{H}}^\perp$ or $\hat{\mathcal{H}}^{zz}$. In order to solve this problem we rewrite the Ising part in Eq. (2.7) and split the Heisenberg Hamiltonian as $\hat{\mathcal{H}} = \hat{\mathcal{H}}_1 + \hat{\mathcal{H}}_2$,

$$\begin{aligned}\hat{\mathcal{H}}_1 &= \sum_i \varepsilon_i \left(\frac{1}{2} - S_i^z \right) + \hat{\mathcal{H}}^\perp, \quad \varepsilon_i = H - \frac{1}{2} \sum_j J_{ij}, \\ \hat{\mathcal{H}}_2 &= \sum_{\langle ij \rangle} J_{ij} \left(\frac{1}{2} - S_i^z \right) \left(\frac{1}{2} - S_j^z \right).\end{aligned}\tag{2.8}$$

Localized states (2.6) are eigenstates of $\hat{\mathcal{H}}_1$ with the eigenvalue $H - 2J$ ($S = 1/2$) and, trivially, of $\hat{\mathcal{H}}_2$ with zero eigenvalue. Then, the proof for the sawtooth chain copies the above arguments for the kagomé antiferromagnet applied to $\hat{\mathcal{H}}_1$ and $\hat{\mathcal{H}}_2$ instead of $\hat{\mathcal{H}}^\perp$ and $\hat{\mathcal{H}}^{zz}$. Similar conclusion has been earlier obtained using a somewhat different approach in Ref. 6).

After establishing that isolated localized magnons are the lowest energy states, the high-field magnetization process of geometrically frustrated spin systems at $T = 0$ can be understood as follows. Above H_s all magnetization subsectors are separated from the ferromagnetic ground state by finite gaps $E_n = n(H - H_s)$. At the saturation field all gaps in subsectors with $n \leq N_{\max}$ vanish and a huge degeneracy of the quantum ground state develops for frustrated antiferromagnets. Below H_s the subsector with the largest possible density of localized magnons $n = N_{\max}$ corresponds to the lowest energy. Therefore, there is a finite jump of the magnetization at $H = H_s$ between a saturated phase and a magnon crystal state. Such universal jumps with $\Delta M = N_{\max}/N$ have been found in numerical exact diagonalization studies of finite clusters of the sawtooth chain, kagomé and checkerboard lattice antiferromagnets and several other frustrated one-dimensional models.^{4), 5), 8)–10)} It is intuitively clear that noninteracting localized magnons being the lowest energy state in the corresponding magnetization subsectors make also the largest contribution to the partition function at low temperatures. Moreover, since the localized excitations have no dynamics their statistics is equivalent to statistics of specially chosen classical particles. Using such a mapping one can find an exact low-temperature behavior of quantum frustrated magnets in the vicinity of the saturation field.⁷⁾ Corrections to such an asymptotic behavior should be exponentially small once the isolated localized magnons are separated from higher-energy propagating states by finite gaps. Below we consider separately the low-temperature properties of the sawtooth chain and kagomé antiferromagnet.

§3. The sawtooth chain

Contribution of degenerate levels to the partition function is determined by dimensionality of the corresponding subspace of the total Hilbert space of a quantum system. In order to calculate the dimensionality we can utilize an arbitrary basis for degenerate states. Such a basis has to be complete but not necessarily orthogonal. Among different configurations of noninteracting localized magnons only states formed by magnons localized in isolated valleys have to be counted for the sawtooth chain. Extended localized states, such as a state on the right-hand-side of Fig. 1, are represented as linear combinations of the basis valley states. The multimagnon ‘valley’ states can be associated with dimer coverings of a base chain: once a localized spin-flip (2·6) occupies a given valley or a site of the base chain it is impossible to put another localized magnon to the same or the adjacent valleys. The hard-dimer states in a given magnetization subsector are linearly independent. This property can be proven by induction using linear independence of the valley states (2·6) in the one-magnon subsector. In the following, we estimate gaps which separate the hard-dimer states from a continuum of the scattering states and then calculate the low-temperature thermodynamics of the sawtooth chain.

3.1. Two-magnon bound states

The scattering states of two magnons can be in principle calculated exactly using a general method discussed in Ref. 11). We shall adopt instead a variational approach, which is much simpler for the present problem. The two branches of single magnon excitations for the sawtooth chain Eq. (2·4) are separated by a finite gap $\Delta\omega = 2JS$. The low-energy scattering states are, therefore, formed by magnons from the lowest branch $\omega_1(k)$. In the two-magnon sector there are $\frac{1}{2}(N/2)(N/2 + 1)$ states constructed from $N/2$ one-magnon states of the dispersionless branch. The number of the basis hard-dimer states is $\frac{1}{2}(N/2)(N/2 - 3)$. The difference between the two yields the number of low-energy scattering states, which is equal to N . In real space representation the above scattering states correspond to localized magnons occupying either the same $|\varphi_i^2\rangle$ or the adjacent $|\varphi_i\varphi_{i+1}\rangle$ valleys. We again assume $S = 1/2$ for simplicity and construct accordingly the following variational basis for the low-energy interacting two-particle states:

$$\begin{aligned} |\psi_i\rangle &= \frac{1}{\sqrt{35}}(S_{1i}^- - 2S_{2i}^- + S_{3i}^-)(S_{1,i+1}^- - 2S_{2,i+1}^- + S_{3,i+1}^-)|0\rangle \simeq |\varphi_i\varphi_{i+1}\rangle \\ |\tilde{\psi}_i\rangle &= \frac{1}{6}(S_{1i}^- - 2S_{2i}^- + S_{3i}^-)^2|0\rangle \simeq |\varphi_i^2\rangle. \end{aligned} \quad (3.1)$$

The exclusion principle of spin-flips has been used for normalization in the above equation. States $|\psi_i\rangle$ and $|\tilde{\psi}_i\rangle$ have nonvanishing overlaps:

$$\langle\psi_i|\psi_{i\pm 1}\rangle = 1/35, \quad \langle\psi_i|\tilde{\psi}_i\rangle = \langle\psi_i|\tilde{\psi}_{i+1}\rangle = \sqrt{5/63}. \quad (3.2)$$

The nonzero matrix elements of the Hamiltonian between these states are

$$\langle\psi_i|\hat{\mathcal{H}}|\psi_i\rangle = 2H - \frac{24}{7}J, \quad \langle\tilde{\psi}_i|\hat{\mathcal{H}}|\tilde{\psi}_i\rangle = 2H - 2J, \quad \langle\psi_{i\pm 1}|\hat{\mathcal{H}}|\psi_i\rangle = \frac{2H - 4J}{\sqrt{35}},$$

$$\langle \tilde{\psi}_{i\pm 1} | \hat{\mathcal{H}} | \tilde{\psi}_i \rangle = \frac{1}{9}J, \quad \langle \tilde{\psi}_i | \hat{\mathcal{H}} | \psi_i \rangle = \langle \tilde{\psi}_{i+1} | \hat{\mathcal{H}} | \psi_i \rangle = \frac{10H - 14J}{3\sqrt{35}}. \quad (3-3)$$

A simple variational ansatz for a propagating state of two localized magnons in adjacent valleys is constructed as $|k\rangle = \sum_i e^{-ikr_i} |\psi_i\rangle$. It has the following energy

$$E(k) = \frac{\langle k | \hat{\mathcal{H}} | k \rangle}{\langle k | k \rangle} = 2(H - 2J) + \frac{20J}{35 + 2 \cos k}. \quad (3-4)$$

Two interacting localized magnons cannot scatter on each other because of an absence of propagating one-particle states at low energies. Instead they form a bound two-magnon pair with energy $E(k)$. Finite dispersion of such pairs comes from assisted hopping of adjacent localized magnons. The minimal value of $E(k)$ is reached at $k = 0$ with the gap $\Delta = 20/37J \approx 0.54J$ separating the low-energy boundary $E_2 = 2(H - 2J)$ from the higher energy states. Numerical minimization of $E(k)$ for an improved variational ansatz $|k\rangle = \sum_i e^{-ikr_i} (|\psi_i\rangle + c|\tilde{\psi}_i\rangle)$ yields $\Delta \approx 0.44J$ with an optimal value $c \approx -0.24$. This value of the gap compares very well with the numerical diagonalization result $0.42J$.⁹⁾ The gap is determined mostly by a nearest-neighbor repulsion of localized magnons in adjacent valleys. The dispersion of bound two-magnon complexes $E(k)$ is weak and does not exceed 7%. We conjecture that the intervalley repulsion leads to a similar behavior in all n -magnon sectors: the lowest energy states with $E_n = n(H - 2J)$ are separated from the scattering states by a finite gap $\Delta_n = O(J)$. At temperatures $T \ll \min_n \{\Delta_n\}$ one can neglect the higher energy states and consider only the contribution of isolated localized magnons. The latter problem is equivalent to a one-dimensional lattice gas of particles with energies $H - 2J$ and on-site and nearest-neighbor exclusion principle, which is also known as a classical hard-dimer model.

3.2. Low-temperature behavior

We consider classical hard dimers on a periodic chain of length $L = N/2$, N being the number of spins in the sawtooth chain. The partition function of this model is

$$\mathcal{Z} = \sum_{\{\sigma\}} \exp \left[\frac{\mu}{T} \sum_i \sigma_i \right] \prod_{\langle ij \rangle} (1 - \sigma_i \sigma_j), \quad (3-5)$$

where $\mu = H_s - H$ is the chemical potential and $\sigma_i = 0, 1$ are the occupation numbers for dimers and $k_B \equiv 1$. The nearest-neighbor exclusion principle is imposed by the last term. The partition function (3-5) can be exactly calculated using the standard transfer matrix approach. In the thermodynamic limit the free energy is determined by the largest eigenvalue of the transfer matrix:

$$\mathcal{F}/N = -\frac{1}{2} T \ln \left(\frac{1}{2} + \sqrt{\frac{1}{4} + e^{\mu/T}} \right). \quad (3-6)$$

The entropy $\mathcal{S} = -\partial \mathcal{F} / \partial T$ depends on external magnetic field and temperature via μ/T :

$$\mathcal{S}/N = \frac{1}{2} \ln \left(1 + \sqrt{1 + 4e^{\mu/T}} \right) - \frac{1}{2} \ln 2 - \frac{\mu}{4T} \left(1 - \frac{1}{\sqrt{1 + 4e^{\mu/T}}} \right). \quad (3-7)$$

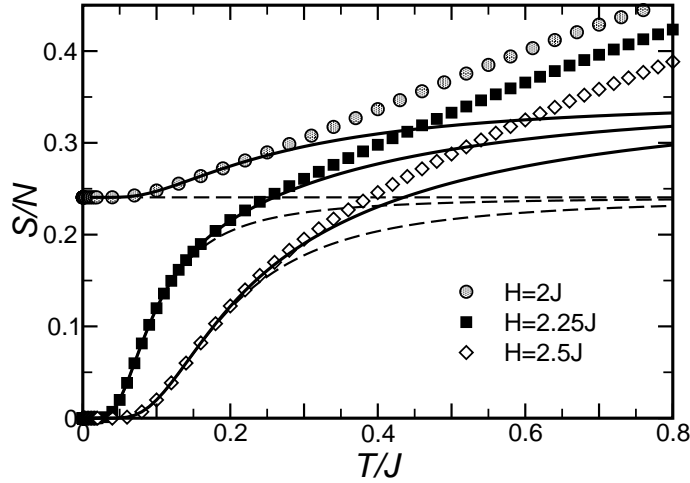


Fig. 3. Temperature dependence of the entropy of the sawtooth chain in magnetic field. Symbols are exact diagonalization data,⁹⁾ dashed lines correspond to the hard-dimer model, solid lines are obtained in the effective Ising model.

During an adiabatic process the combination $(H - H_s)/T$ remains constant and, consequently, temperature drops to zero as $H \rightarrow H_s$. Such a very strong magnetocaloric effect is a direct consequence of the condensation of a macroscopic number of soft modes at $H = H_s$.¹⁶⁾ At $H = H_s$ the entropy remains finite down to $T = 0$ and has a universal value:

$$S/N = \frac{1}{2} \ln \left(\frac{1 + \sqrt{5}}{2} \right) \approx 0.34712 \ln 2. \quad (3.8)$$

The localized magnons of the sawtooth chain behave, therefore, similar to paramagnetic degrees of freedom in an effective field $h = H - H_s$. The major difference with an ideal paramagnet is that the entropy of the latter at $h = 0$ depends on a spin length, whereas the residual entropy of frustrated magnets at $H = H_s$ has a geometric origin.

Using the transfer matrix technique, one can also calculate the dimer-dimer correlation function. The result is

$$\langle \sigma_i \sigma_j \rangle = \bar{\sigma}^2 + (-1)^{i-j} \bar{\sigma} (1 - \bar{\sigma}) e^{-|r_i - r_j|/\xi}, \quad (3.9)$$

where the average dimer density $\bar{\sigma}$ and the correlation length ξ are given by

$$\begin{aligned} \bar{\sigma} &= \sin^2 \frac{\gamma}{2} = \frac{2e^{\mu/T}}{1 + 4e^{\mu/T} + \sqrt{1 + 4e^{\mu/T}}}, & \tan \gamma &\equiv 2e^{\mu/2T} \\ \frac{1}{\xi} &= 2 \log \left(\cot \frac{\gamma}{2} \right) = \log \left(\frac{\sqrt{1 + 4e^{\mu/T}} + 1}{\sqrt{1 + 4e^{\mu/T}} - 1} \right). \end{aligned} \quad (3.10)$$

The correlation length exponentially diverges $\xi \sim e^{\mu/2T}$ as $T \rightarrow 0$.

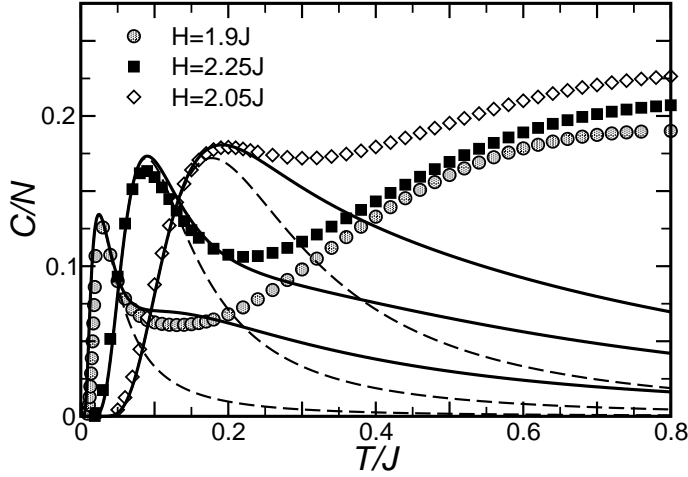


Fig. 4. Temperature dependence of the specific heat of the sawtooth chain in magnetic field. Symbols are exact diagonalization data,⁹⁾ dashed lines correspond to the hard-dimer model, solid lines are obtained in the effective Ising model.

The specific heat is obtained by taking temperature derivative of the internal energy $\mathcal{E} = -1/2 \mu \bar{\sigma}$:

$$C/N = \frac{\mu^2}{8T^2} \sin^2 \gamma \cos \gamma = \frac{\mu^2}{2T^2} \frac{e^{\mu/T}}{(1 + 4e^{\mu/T})^{3/2}}. \quad (3.11)$$

The specific heat as a function of $x = \mu/T$ has two peaks at $x = x_{\pm}$ determined by solutions of the following equation:

$$x + 2 = 2e^x(x - 4) \quad \text{for } x_+ = 4.0526, \quad x_- = -2.8159. \quad (3.12)$$

Comparison of the entropy and the specific heat of the sawtooth chain calculated in the hard-dimer model and by a full numerical diagonalization of a cluster with $N = 20$ sites⁹⁾ is shown in Figs. 3–5. The analytic and the numerical results agree well with each other below $T^* \sim 0.1J$. In particular, the hard-dimer representation correctly reproduces the residual entropy at $H = H_s$ (Fig. 3). At $T > 0.1J$ a thermal contribution of the higher energy states becomes significant. Those states can be partially taken into account by using analogy with Ising models near the saturation field, which are also mapped to statistical models of hard-core objects.^{17),18)} For the sawtooth chain such a generalized Ising representation can be constructed because of a weak dispersion of bound two magnon pairs (3.4). Once the k -dependence of $E(k)$ is ignored, there are no zero-point fluctuations and we end up again with a model of classical hard-core particles, where the nearest-neighbor exclusion is replaced by an Ising type repulsion:

$$\mathcal{H} = \sum_i (-\mu \sigma_i + V \sigma_i \sigma_{i+1}), \quad \sigma_i = 0, 1. \quad (3.13)$$

For the strength of the Ising interaction we have to choose the gap, which separates bound two-magnon pairs from noninteracting localized magnons: $V = \Delta \approx 0.44J$.

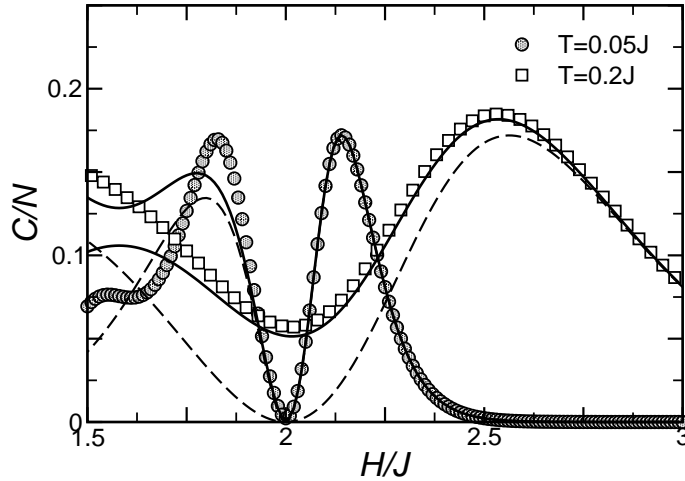


Fig. 5. Field dependence of the specific heat of the sawtooth chain. Symbols are numerical data,⁹⁾ dashed lines correspond to the hard-dimer model, full curves are calculated in the effective Ising model.

The classical Ising model (3-13) is solved exactly by the transfer-matrix method with the following result for the free energy:

$$\mathcal{F}/N = -\frac{1}{2}T \ln \left(\frac{1}{2} [1 + e^{-(V-\mu)/T}] + \sqrt{\frac{1}{4} [1 - e^{-(V-\mu)/T}]^2 + e^{\mu/T}} \right). \quad (3-14)$$

The above expression transforms into the hard-dimer result (3-6) for $T \ll V$. Comparison between numerical exact diagonalization results and the two analytic approximations is presented in Fig. 3. The entropy calculated in the Ising model shows a nice agreement with the numerical data up to a remarkably high $T^* \sim 0.3J$. Note, that the Ising repulsion V is not a fitting parameter, but has been calculated above.

The specific heat of the sawtooth chain as a function of temperature in a constant magnetic field $H \sim H_s$ (Fig. 4) has a peak at $T_m = (H_s - H)/x_{\pm}$, where \pm correspond to $H < H_s$ and $H > H_s$, respectively. Such a low-temperature peak appears due to a freezing of localized degrees of freedom and is well described by both analytic approaches. At higher temperatures $T \sim J$, the specific heat has a second peak, which reflects development of one-dimensional short-range spin correlations. Its presence is not captured, of course, by the low-temperature hard-dimer mapping. Experimental observation of the double-peak structure in temperature dependence of the specific heat of real frustrated magnetic compounds can be a clear sign of localized magnons.

Field dependence of the specific heat is presented in Fig. 5. $C(H)$ has a deep minimum at the saturation field. The minimum occurs due to a weak temperature dependence of $\mathcal{S}(T, H_s)$, which is completely T -independent in the hard-dimer model. According to Eq. (3-12), the high- and low-field peaks in the specific heat correspond to $H_m = H_s - Tx_{\pm}$. Comparison between the three types of the results for the specific heat shown in Fig. 5 allows also to determine the field range, where the localized magnons play a dominant role: $H > 0.8H_s$.

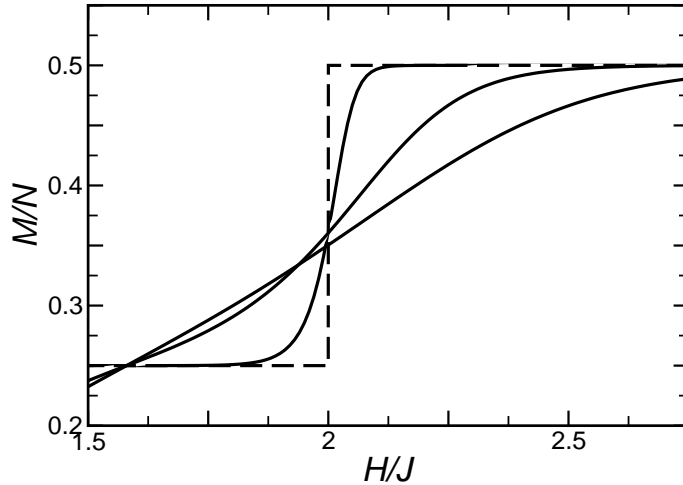


Fig. 6. Magnetization curves of the sawtooth chain obtained in the effective Ising model. Full lines correspond from top to bottom to $T = 0.02J$, $0.05J$, $0.1J$, and $0.2J$; dashed line is the zero-temperature magnetization jump.

The zero-temperature jump between a half-magnetization plateau and the fully saturated phase is smeared at finite temperatures. According to the hard-dimer representation, the magnetization curves $M(H, T) = (1 - \bar{\sigma})/2$ cross at $H = H_s$ with the universal value $M(T, H_s)/N = (1 + \sqrt{5})/4\sqrt{5}$. The finite-temperature width of the jump is approximately $\Delta H \sim 4T$. The above value of the magnetization corresponds to an average density $n = (\sqrt{5} - 1)/4\sqrt{5} \approx 0.1382$ of localized magnons. Magnetization curves of the sawtooth chain are illustrated in Fig. 6 by using the effective Ising model, which give more accurate results for the selected temperatures than the hard-dimer mapping.

§4. Kagomé antiferromagnet

Following our analysis of the sawtooth chain, we define a class of hard-hexagon states for a kagomé antiferromagnet near the saturation. They are built from magnons localized on smallest hexagon voids of a kagomé lattice, such that no two hexagons have common sites. The hard-hexagon states are linearly independent in the thermodynamic limit with at most one linear relation in every magnetization subsector. The centers of hexagons form a triangular lattice and the above states are, therefore, mapped onto a classical gas of hard-core particles on a triangular lattice with the nearest-neighbor exclusion principle. The latter is a famous exactly solvable model¹⁸⁾ and, therefore, a great deal of the exact information is known about such states. However, in order to apply the available results to a kagomé antiferromagnet we first have to show that (i) the hard-hexagon states are separated by finite gaps from the higher-energy states and (ii) there are no other low-energy states in every magnetization subsector with $n \leq N_{\max}$ or their contribution is vanishingly small.

4.1. Two-magnon bound states

Low energy part of the two-magnon subsector of a kagomé antiferromagnet consists of $\frac{1}{2}(N/3)(N/3+1)$ states constructed from one-particle states of the flat branch $\omega_1(\mathbf{k})$. These include $\frac{1}{2}(N/3)(N/3-7)$ hard-hexagon states. Additional $4N/3$ interacting or scattering states correspond to N states of localized magnons, which occupy adjacent hexagons, $|\varphi_i\varphi_{i+a_l}\rangle$, and to $N/3$ states with two spin flips on the same hexagon, $|\varphi_i^2\rangle$. In a simple treatment of a spin-1/2 model we neglect the latter states and define the following real-space basis for the former N states:

$$|\psi_{li}\rangle = \frac{1}{\sqrt{35}} \sum_{n,n'=1}^6 (-1)^{n+n'} S_{ni}^- S_{n'i+a_l}^- |0\rangle, \quad (4.1)$$

where $l = 1-3$ and $\mathbf{a}_1 = (1, 0)$ and $\mathbf{a}_{2,3} = (\pm 1/2, \sqrt{3}/2)$ are three nearest-neighbor sites on a triangular lattice of hexagons. The normalization factor in Eq. (4.1) takes into account the exclusion principle of spin flips. The overlap matrix elements for the above states are

$$\langle\psi_{2i}|\psi_{1i}\rangle = -1/7, \quad \langle\psi_{3i}|\psi_{1i}\rangle = \langle\psi_{li\pm a_{l'}}|\psi_{li}\rangle = 1/35. \quad (4.2)$$

The Hamiltonian (2.1) has the following nonzero matrix elements

$$\langle\psi_{1i}|\hat{\mathcal{H}}|\psi_{1i}\rangle = 2H - \frac{40}{7}J, \quad \langle\psi_{2i}|\hat{\mathcal{H}}|\psi_{1i}\rangle = -\frac{10H - 29J}{35}, \quad \langle\psi_{3i}|\hat{\mathcal{H}}|\psi_{1i}\rangle = \frac{2H - 6J}{35}. \quad (4.3)$$

All other nonvanishing matrix elements are obtained from Eqs. (4.2) and (4.3) by applying symmetry operations of a kagomé lattice. Using ansatz $|\mathbf{k}\rangle = \sum_{il} e^{-i\mathbf{k}\cdot\mathbf{r}_i} c_l |\psi_{li}\rangle$ for a bound state of two magnons we calculate its energy as

$$E(\mathbf{k}) = \frac{\langle\mathbf{k}|\hat{\mathcal{H}}|\mathbf{k}\rangle}{\langle\mathbf{k}|\mathbf{k}\rangle} = 2(H - 3J) + \varepsilon(\mathbf{k}), \quad (4.4)$$

$$\varepsilon(\mathbf{k}) = \frac{2}{7} \frac{|c_1|^2 + |c_2|^2 + |c_3|^2 - \frac{1}{10}P_{\mathbf{k}}}{(|c_1|^2 + |c_2|^2 + |c_3|^2)[1 + \frac{2}{35}(\cos k_1 + \cos k_2 + \cos k_3)] - \frac{1}{7}P_{\mathbf{k}} + \frac{1}{35}Q_{\mathbf{k}}},$$

$$P_{\mathbf{k}} = c_1 c_2^*(1 + e^{-ik_3}) + c_2 c_3^*(1 + e^{ik_1}) + c_3 c_1^*(e^{-ik_1} + e^{ik_3}) + \text{c. c.},$$

$$Q_{\mathbf{k}} = c_1 c_2^*(e^{ik_1} + e^{-ik_2}) + c_2 c_3^*(e^{ik_2} + e^{-ik_3}) + c_3 c_1^*(1 + e^{i(k_3 - k_1)}) + \text{c. c.},$$

where $k_i = \mathbf{k} \cdot \mathbf{a}_i$. The minimum of $\varepsilon(\mathbf{k})$ occurs at zero total momentum $\mathbf{k} = 0$ for $c_1 = c_2 = c_3$ with a gap $\Delta = 0.24J$. This value of the gap can be again used as an estimate for the repulsion between localized magnons on adjacent hexagons, though dispersion of bound pairs $\sim 12\%$ is somewhat larger in two dimensions.

Among various states of n isolated localized magnons there are also states, which do not obey the hard-hexagon rules. The simplest example of such a ‘defect’ state is shown in Fig. 7: two localized magnons reside on a small $|\varphi_i\rangle$ and a large $|\varphi_L\rangle$ hexagons. The large hexagon state is decomposed into a basis hexagon states (2.5) as

$$|\varphi_L\rangle = \sum_{l=1}^6 |\varphi_{i+a_l}\rangle + |\varphi_i\rangle. \quad (4.5)$$

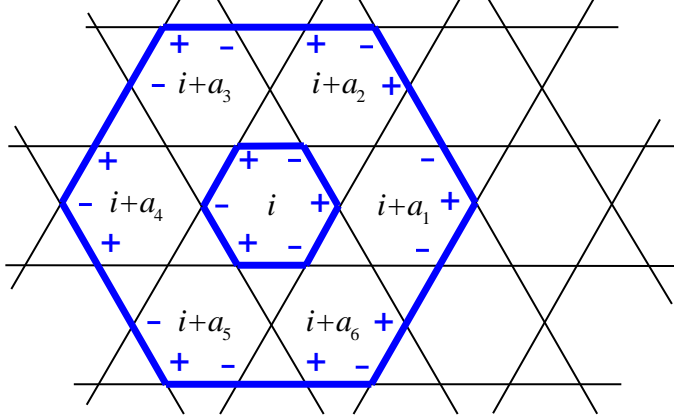


Fig. 7. The defect state of two localized magnons, which breaks the hard-hexagon rule.

The two-particle state $|\varphi_L\varphi_i\rangle$ corresponds, therefore, to a special linear combination of states (4.1) and state $|\varphi_i^2\rangle$ and, obviously, breaks the hard-hexagon rules. By analogy with Fig. 7 a general defect two-magnon state $|\varphi_L\varphi_{L'}\rangle$ is constructed by drawing two closed lines L and L' on a kagomé lattice such that (i) the lines can host localized magnons and (ii) one of the lines L' lies inside the area A_L enclosed by the second line: $L' \subset A_L$. Such states are, however, topologically equivalent to the two-magnon state in Fig. 7 and can be represented as linear combinations of normal hard-hexagon states and the primitive defect state. In addition, if one or both lines L and L' have nonzero winding around the cluster, the corresponding two-magnon state cannot again be decomposed into hard-hexagon states (see discussion in Sec. 2). In the two-magnon subsector the total number of states breaking the hard-hexagon rule is $\propto N$, that is a factor of $1/N$ smaller than the number of hard-hexagon states. Similar estimate holds for the three-magnon subsector: $O(N^2)$ defect states versus $O(N^3)$ hard-hexagon states and so on. In addition, in magnetization subsectors with finite densities of magnons the number of defect states is further reduced. Indeed, the defect state shown in Fig. 7 exists only if there are no localized magnons on any of 12 small hexagons surrounding the larger loop. As the total density n/N of (localized) magnons grows, there is less and less space for the composite defect states. Finally, if there are more than two magnons on every 19 hexagons or $n/N > 2/(19 \cdot 3) \approx 0.035$, the number of defect states becomes significantly suppressed and eventually goes to zero.

Another complication for the kagomé antiferromagnet comes from the fact that the gap for one of the dispersive branches in Eq. (2.2) also vanishes at the saturation field. The corresponding propagating magnon has the same energy $\omega_3(0) = H - 3J$ as localized magnons from the flat branch. The lowest-energy states in the two-magnon subsector contain apart from the isolated localized magnons also superposition states

of one localized magnon and one propagating magnon. Such states form a continuum above the low-energy threshold $E_2 = 2(H - 3J)$. The same is true for all n -magnon subsectors with $n \ll N$. Once n becomes a finite fraction of N the above picture changes. The low-energy propagating magnons experience multiple scattering from an infinite number of localized magnons. Such scattering produces a finite shift of the energy of propagating magnons. An exact value of energy shift for $\omega_3(\mathbf{k})$ depends on a precise pattern of localized magnons. An explicit estimate can be obtained for an average ‘uniform’ state of n -localized magnons, corresponding to a low-temperature ensemble of states with different translational patterns. We bosonize the spin Hamiltonian using, *e.g.*, the Dyson-Maleev transformation: $S_i^+ = \sqrt{2S}(1 - b_i^\dagger b_i/2S)b_i$, $S_i^- = \sqrt{2S}b_i^\dagger$, for an arbitrary value of on-site spin S . Diagonalization of quadratic terms gives the excitation spectrum (2.2). Effect of interaction between magnons is treated in the lowest order by using the Hartree-Fock approximation. We define two averages: for an on-site density $m_1 = \langle b_i^\dagger b_i \rangle$ and for a nearest-neighbor hopping $m_2 = \langle b_i^\dagger b_j \rangle$. After a mean-field decoupling of four-boson terms the effect of interaction is reduced to a renormalization $S \rightarrow (S - m_1 + m_2)$ in the quadratic terms. The lowest point of the dispersive branch is at $\omega_3(0) = H - 6J(S - m_1 + m_2)$, which reduces at the saturation field $H_s = 6JS$ to $\Delta_d = 6J(m_1 - m_2)$. For a single localized magnon (2.5) one finds $m_1 = -m_2 = 1/6$. Hence, the dispersive mode propagating through an ‘averaged ensemble’ of n localized magnons acquires a finite gap $\Delta_d = 3Jn/N$, which separates the dispersive branch from the localized magnons. At low enough temperatures $T \ll \Delta_d$ the dispersive modes have a negligible contribution to the thermodynamics of a kagomé antiferromagnet. Note, that characteristic temperature, where the above approximation becomes valid, depends on an average density of magnons and, therefore, on an applied magnetic field.

4.2. Low-temperature behavior

In the above analysis we have established that the hard-hexagon description of lowest energy states is valid at sufficiently high densities of magnons. High or low means here in comparison to the density of the magnon crystal: $n/N = 1/9$. Let us now discuss the thermodynamic properties of a spin-1/2 kagomé antiferromagnet in the hard-hexagon approximation. The partition function of the hard-hexagon lattice gas is given by the same expression (3.5), where the site index runs over $\mathcal{N} = N/3$ sites of a triangular lattice formed by centers of hexagon voids of the original kagomé lattice. This model was solved by Baxter with the help of a corner transfer matrix method.¹⁸⁾ Specifically, the normalized partition function $\mathcal{Z}^{1/\mathcal{N}}$ and the fugacity $z = e^{\mu/T}$ are expressed as functions of a real auxiliary parameter x : at the high-field region $0 < z < z_c$ ($-1 < x < 0$),

$$z = -x \frac{H^5(x)}{G^5(x)}, \quad H(x) = \prod_{n=1}^{\infty} [(1 - x^{5n-4})(1 - x^{5n-1})]^{-1}, \quad (4.6)$$

$$G(x) = \prod_{n=1}^{\infty} [(1 - x^{5n-3})(1 - x^{5n-2})]^{-1}, \quad Q(x) = \prod_{n=1}^{\infty} (1 - x^n),$$

$$\mathcal{Z}^{1/N} = \frac{H^3(x)Q^2(x^5)}{G^2(x)} \prod_{n=1}^{\infty} \frac{(1-x^{6n-4})(1-x^{6n-3})^2(1-x^{6n-2})}{(1-x^{6n-5})(1-x^{6n-1})(1-x^{6n})^2};$$

whereas at the low-field region $z > z_c$ ($0 < x < 1$),

$$z = x^{-1} \frac{G^5(x)}{H^5(x)}, \quad R(x) = \frac{Q(x)Q(x^5)}{Q^2(x^3)}, \quad (4.7)$$

$$\mathcal{Z}^{1/N} = \frac{x^{-1/3}G^3(x)Q^2(x^5)}{H^2(x)} \prod_{n=1}^{\infty} \frac{(1-x^{3n-2})(1-x^{3n-1})}{(1-x^{3n})^2}.$$

A nonanalytic behavior of the partition function at $z = z_c = (11+5\sqrt{5})/2 \approx 11.09017$ as $x \rightarrow \pm 1$ indicates presence of a critical point. Such a continuous order-disorder transition corresponds to a spontaneous occupation of one of the three triangular sublattices at high densities. Expansion of \mathcal{Z} in powers of $z - z_c$ yields exact critical exponents of the hard-hexagon model,¹⁸⁾ whereas numerical evaluation of rapidly converging infinite products provides dependence of various physical quantities on the chemical potential (temperature).

Low-temperature behavior of a spin-1/2 kagomé in the vicinity of the saturation field can be obtained from the above exact solution by a trivial rescaling from the number of hexagons to the number of spins and using the relation $\mu = H_s - H$. The entropy as a function of magnetic field at constant T reaches a sharp maximum at $H = H_s$. At the saturation field ($z = 1$, $x = -0.25496$) both the entropy and the magnetization have universal temperature independent values:

$$S_s/N = 0.11108 \approx 0.16026 \ln 2, \quad M_s/N = 0.44596. \quad (4.8)$$

The above value of the magnetization corresponds to the density $n_s/N \approx 0.054$ of localized magnons. This density well exceeds an estimate $n \sim 0.035$ from the previous subsection, which signifies suppression of the non-hard-hexagon states. As an external field is further decreased there is a continuous crystallization transition into a close-packed structure (Fig. 2) with broken translational symmetry. The transition takes place at a temperature dependent critical field $H_c(T)$:

$$H_c(T) = H_s - T \ln z_c \approx 3J - 2.40606T, \quad (4.9)$$

whereas the magnetization has again a universal value:

$$M_c/N = 1/2 - 1/3 \rho_c, \quad \rho_c = (5 - \sqrt{5})/10. \quad (4.10)$$

The density of magnons at the transition point $n_c/N = \rho_c/3 \approx 0.0921$ is about 20% smaller than the density of the ideal close-packed structure $n/N = 1/9$. The second order transition at $H_c(T)$ belongs to the universality class of a two-dimensional three-state Potts model¹⁹⁾ and has the following exact critical exponents: $\alpha = 1/3$, $\beta = 1/9$, $\gamma = 13/9$, and $\nu = 5/6$.¹⁸⁾ The uniform susceptibility $\chi = \partial M/\partial H$ also diverges at the transition point with the same critical exponent α as the specific heat. Apart from a sharp lambda-peak at $z = z_c$, the specific heat has also a rounded Schottky type anomaly at $z_m = 0.03897$ ($x = -0.03296$, $\ln z_m = -3.24502$).

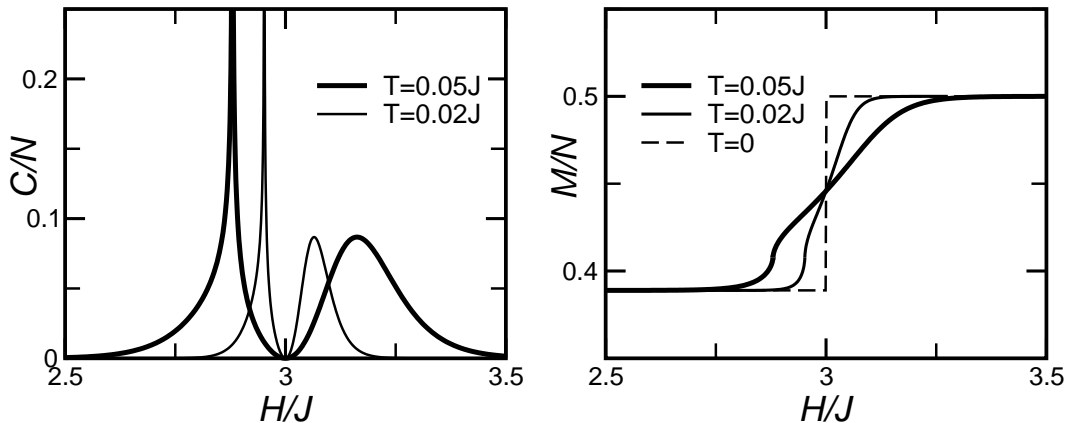


Fig. 8. Field dependence of the specific heat (left) and the magnetization (right) of a spin-1/2 kagomé antiferromagnet obtained in the hard-hexagon model.

Hard-hexagon results for the field dependence of the specific heat and the magnetization of a spin-1/2 kagomé antiferromagnet are shown in Fig. 8. Positions of two peaks in the specific heat scale linearly with temperature. As a function of temperature at a fixed magnetic field the specific heat also exhibits a characteristic low-temperature peak at $T_m = (H_s - H)/\ln z_m$, see Fig. 9. At higher temperatures $T \sim J$ there should be a second maximum in $C(T)$, which is not captured by hard-hexagon mapping and corresponds to development of short-range spin correlations. Overall, the behavior of the specific heat and the magnetization of a kagomé antiferromagnet resembles the previous results for the sawtooth chain. The major difference is that while one-dimensional model has only a finite temperature crossover, in two-dimensions the breaking of a discrete translational symmetry occurs via a sharp second-order transition. Experimental observations of a double peak structure in a temperature (field) dependence of the specific heat and of a characteristic non-monotonic temperature dependence of the magnetization (Fig. 9, right panel) could be a clear signature of degenerate magnons in a geometrically frustrated magnetic material.

Since the gaps between the noninteracting localized magnons and propagating states are smaller for a kagomé antiferromagnet, the quantitative validity of the hard-hexagon mapping is restricted to lower temperatures $T < 0.05-0.1J$ and to higher magnetic fields $H > 0.9H_s$. The critical behavior obtained from the exact solution for hard hexagons should, however, remain valid even beyond the above range. At present there are no numerical results on the magnetothermodynamics of a spin-1/2 kagomé antiferromagnet in order to compare them with the hard-hexagon mapping. Note, that exact diagonalization results on finite periodic clusters should suffer from rather strong finite size effects. They are determined by a presence of large number of non-hard-hexagon states of localized magnons, such as the ‘defect’ states discussed earlier in this section, whose contribution vanishes only in the thermodynamic limit $N \rightarrow \infty$.

The order parameter of the hard-hexagon model is defined as a difference of

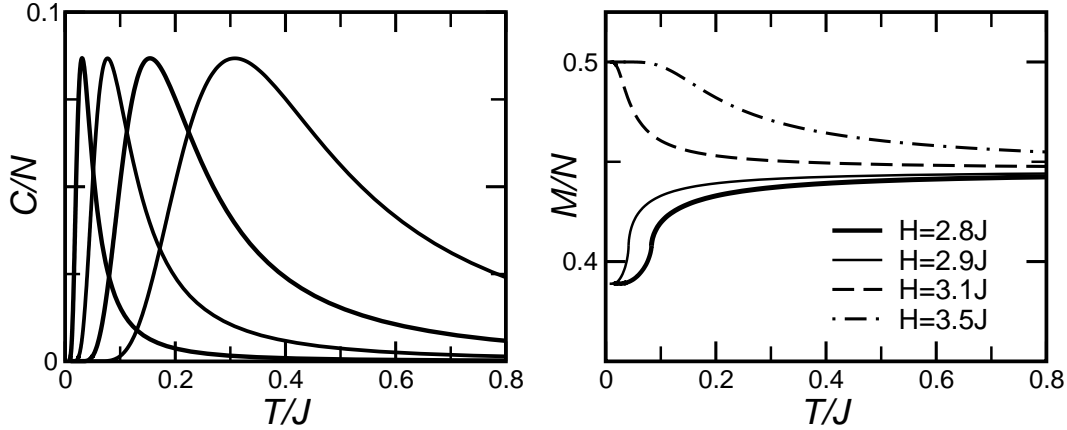


Fig. 9. Temperature dependence of the specific heat (left) and the magnetization (right) of a spin-1/2 kagomé antiferromagnet obtained in the hard-hexagon model. Curves on the left panel correspond to $H = 3.1J, 3.25J, 3.5J,$ and $4J$ from left to right.

hexagon densities ρ_i on adjacent sites: $R = \rho_i - \rho_{i+a}$.¹⁸⁾ Up to a renormalization prefactor R is equal to the Fourier harmonics $\rho_{\mathbf{q}}$ at $\mathbf{q} = (4\pi/3a^*, 0)$, where a^* is a period of a triangular lattice. In a kagomé antiferromagnet the magnon crystal has two types of spins, on hexagons with localized magnons and between them. The two sublattices have different average magnetizations: $\langle S^z \rangle = 1/3$ and $1/2$ at $T = 0$. Hence, the crystalline order of magnons reveals itself as an extra Fourier harmonics in the magnetic structure factor $S^{zz}(\mathbf{q})$. The wave-vector of magnon crystal is the same one as for a so-called $\sqrt{3} \times \sqrt{3}$ structure, stabilized in zero field for a kagomé antiferromagnet with large $S \gg 1$.²⁰⁾ Note, that the magnon crystal state is not reduced to a semiclassical collinear two-sublattice order. The quantum coherence of spin-flip propagating around one hexagon plays a crucial role in stabilizing the magnon crystal.

Finally, the schematic phase diagram of a Heisenberg spin-1/2 kagomé antiferromagnet in external magnetic field is shown in Fig. 10. In zero magnetic field this quantum frustrated model has a nonmagnetic ground state with a large number of low-lying singlet excitations between the ground state and the lowest excited triplet.^{21), 22)} Presence or absence of a finite-temperature phase transition at $H = 0$ depends on whether such a singlet ground state is a valence bond crystal, which breaks certain discrete lattice symmetries, or a true spin-liquid state with full symmetry of the Heisenberg Hamiltonian. The answer to this question is not known at present due to a limited size of clusters accessible for numerical diagonalization. Applied magnetic field eventually closes the triplet gap and the system transforms into a state with finite magnetization. Numerical investigations of the magnetization curve of a spin-1/2 Heisenberg model find a clear plateau at $1/3$ of the saturation magnetization.^{23), 24)} The ground state at the $1/3$ -plateau has a long-range order of valence-bond type with the same $\sqrt{3} \times \sqrt{3}$ periodicity as the magnon crystal in Fig. 2.²⁵⁾ There is, therefore, a line of phase transitions, which separates the $1/3$ plateau state from a paramagnetic phase and phases above and below the plateau.

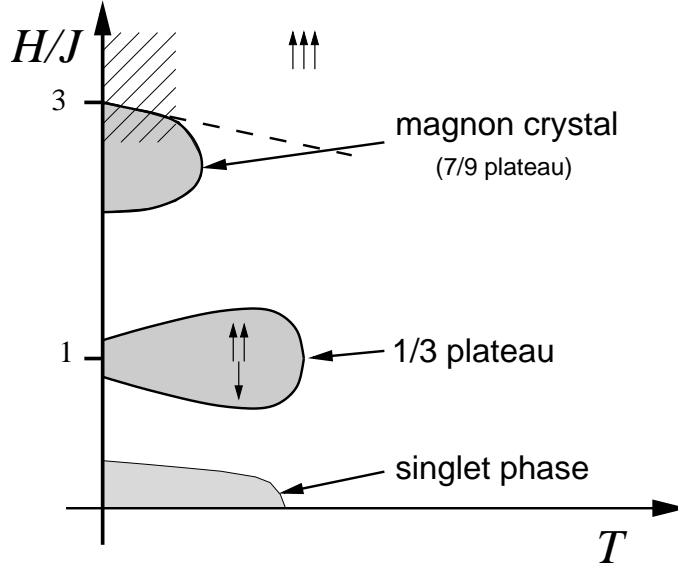


Fig. 10. Schematic H - T phase diagram of a Heisenberg spin-1/2 kagomé antiferromagnet. Dashed area shows a region of applicability of the hard-hexagon mapping.

The magnon crystal state is the third presently known phase of a spin-1/2 kagomé antiferromagnet, which is stabilized in the vicinity of the saturation field. At zero temperature the magnon crystal corresponds to the 7/9-magnetization plateau. The hard-hexagon mapping obtained in Ref. 7) and further developed in the present work is valid in the dashed region of the phase diagram. Being restricted to high fields and low temperatures the hard-hexagon mapping is, nevertheless, quite important, since it provides the only exact information about the phase diagram of a spin-1/2 Heisenberg antiferromagnet on a kagomé lattice.

Between the above three phases, magnetization of a kagomé antiferromagnet grows continuously,^{23),24)} which points at a gapless excitation spectrum. The number and the nature of such intermediate phases remain an open issue. Gapless states with finite magnetization can also have nontrivial properties and exotic order parameters even in the classical limit $S \rightarrow \infty$.²⁶⁾

§5. Discussion

The above analysis of the magnetothermodynamics of the sawtooth chain and of the quantum kagomé antiferromagnet has been focused mainly on spin-1/2 models. Apart from a detailed presentation of the previous results^{4),6),7)} we have developed an effective Ising description of localized magnons for the sawtooth chain, which is valid up to significantly higher temperatures than the hard-dimer approximation. Most of the discussed results remain valid for an arbitrary quantum spin S . These include the universal values of the entropy at $H = H_s$ and the finite temperature transition into the magnon crystal state for a kagomé lattice model. The zero temperature magnetization jumps become, however, increasingly small for large

S : a relative height of the jump decreases as $\Delta M = 1/(9S)$ for a kagomé antiferromagnet. The temperature range for stability of the magnon crystal also becomes smaller with increasing S . Indeed, the gap between localized magnon states and higher-energy propagating states is proportional to the exchange constant J . (Variational calculations for the $S = 1$ sawtooth chain yield only a slightly different gap $\Delta = 0.41J$ compared to the $S = 1/2$ result of Sec. 3.) The crystallization temperature scales, therefore, as $T_c = O(J)$ and becomes a small fraction of the Curie-Weiss constant $T_c/\theta_{CW} \sim 1/S^2$. The domain of quantum effects is pushed to extremely low temperatures for semiclassical spins $S \gg 1$.

A strong magnetocaloric effect discussed in Sec. 3 remains, however, present even in the classical limit $S \rightarrow \infty$.¹⁶⁾ Recently, a large temperature decrease during an adiabatic demagnetization process has been measured in pyrochlore compound $\text{Gd}_2\text{Ti}_2\text{O}_7$ with $S = 7/2$.²⁷⁾ Note, that antiferromagnets on a pyrochlore and a checkerboard lattices also have localized magnon excitations. Their low-temperature behavior is, therefore, mapped to lattice gas models of hard-core classical particles. For the checkerboard antiferromagnet an appropriate low-temperature model is a square lattice gas of hard-core particles with nearest- and next-nearest neighbor exclusions. There is no exact solution for such statistical model. Still, effective representations may be quite useful, because lattice gas models can be efficiently studied with a powerful classical Monte Carlo method. The thermodynamics of the corresponding lattice models generally depends on a dimensionless fugacity $z = e^{(H_s - H)/T}$. This immediately implies a strong magnetocaloric effect $T \rightarrow 0$ as $H \rightarrow H_s$ for all frustrated magnets with localized spin-flips. The residual entropy at $H = H_s$, which determines a cooling power, does depend on a lattice geometry. An interesting open problem is calculation of the residual entropies for pyrochlore and checkerboard antiferromagnets in order to determine the favorable geometrically frustrated spin system for applications in adiabatic refrigerators.^{28),29)} There is also a certain difference in the magnetocaloric effect for quantum and (semi)classical frustrated magnets. The quantum spin systems exhibit a strong cooling on the two sides of the saturation field when $H \rightarrow H_s \pm 0$: both the saturated phase at $H > H_s$ and the magnon crystal at $H < H_s$ have no entropy at $T = 0$. Frustrated classical spin system has in contrast infinite degeneracy of the ground state for $H < H_s$. Therefore, a much stronger cooling effect is found when applied field is decreased towards H_s from the high-field side.¹⁶⁾ For intermediate values of spin $S > 1$ the quantum order by disorder effect³⁰⁾ lifts the classical degeneracy at $H < H_s$ and restores zero entropy. This leads to an asymmetric field dependence for $T_S(H)$ with the steepest slope at $H > H_s$ and the lowest temperature achievable in the vicinity of the saturation field.

Real magnetic materials usually have additional weak interactions apart from a nearest-neighbor Heisenberg exchange. These include, for example, various anisotropies, next-nearest-neighbor exchanges, and the dipolar interactions. Such extra interactions lift the classical degeneracy of frustrated magnets and in the quantum case induce a weak dispersion of the lowest magnon branches (2·2) and (2·4). Phase transition at $H = H_s$ corresponds, then, to a usual condensation of a single magnon mode at a certain wave-vector \mathbf{Q} . The finite zero-temperature entropy at

the saturation field is completely destroyed in such a case. The question, whether some of the effects described in the present paper are still observable or not, can be solved by a simple comparison of the energy scales. If the gap in a magnon crystal state exceeds the bandwidth W of the lowest branch $\omega_1(\mathbf{k})$, then there has to be a subsequent phase transition between a state with transverse magnetic order in the immediate vicinity of H_s and the crystal state without such ordering. (There will be, of course, zero-point fluctuations in the magnon crystal ground state on top of a simple product of localized magnon wave-functions, Fig. 2.) As long as the energy scale for weak residual interactions is significantly smaller than the nearest-neighbor exchange $W \ll J$, a frustrated magnet continues to exhibit a large magnetocaloric effect. The lowest reachable temperature is, however, limited to $T_{\min} \sim W$. Finally, one of the suitable ways to detect experimentally nearly dispersionless magnon bands in frustrated magnets is to measure a low-temperature peak in the specific heat for $T_m = (H - H_s)/\ln z_m > W$.

Acknowledgments

We are grateful to A. Honecker for providing us the numerical data for the sawtooth chain. H. T. is supported by a Grant-in-Aid from the Ministry of Education, Science, Sports, and Culture of Japan.

References

- 1) A. P. Ramirez, B. S. Shastry, A. Hayashi, J. J. Krajewski, D. A. Huse, and R. J. Cava, Phys. Rev. Lett. **89** (2002), 067202.
- 2) S. Hov, H. Bratsberg, and A. T. Skjeltorp, J. Magn. Magn. Mater. **15–18** (1980), 455.
- 3) H. Ueda, H. A. Katori, H. Mitamura, T. Goto, and H. Takagi, Phys. Rev. Lett. **94** (2005), 047202.
- 4) J. Schulenburg, A. Honecker, J. Schnack, J. Richter, and H.-J. Schmidt, Phys. Rev. Lett. **88** (2002), 167207.
- 5) J. Schnack, H.-J. Schmidt, J. Richter, and J. Schulenburg, Eur. Phys. J. B **24** (2001), 475.
- 6) H.-J. Schmidt, J. Phys. A **35** (2002), 6545.
- 7) M. E. Zhitomirsky and H. Tsunetsugu, Phys. Rev. B **70** (2004), 100403.
- 8) J. Richter, J. Schulenburg, A. Honecker, J. Schnack, and H.-J. Schmidt, J. Phys.: Condens. Matter **16** (2004), S779.
- 9) M. E. Zhitomirsky and A. Honecker, J. Stat. Mech.: Theor. Exp. (2004), P07012.
- 10) O. Derzhko and J. Richter, Phys. Rev. B **70** (2004), 104415.
- 11) D. C. Mattis, *The Theory of Magnetism I* (Springer, Berlin, 1981).
- 12) E. G. Batyev and L. S. Braginskii, Zh. Éksp. Teor. Fiz. **87** (1984), 1361 [Sov. Phys. JETP **60** (1984), 781].
- 13) G. Jackeli and M. E. Zhitomirsky, Phys. Rev. Lett. **93** (2004), 017201.
- 14) A. P. Ramirez, G. P. Espinosa and A. S. Cooper, Phys. Rev. B **45** (1992), 2505.
- 15) K. Isawa, Y. Yaegashi, M. Komatsu, M. Nagano, S. Sudo, M. Karppinen, and H. Yamauchi, Phys. Rev. B **56** (1997), 3457.
- 16) M. E. Zhitomirsky, Phys. Rev. B **67** (2003), 104421.
- 17) B. D. Metcalf and C. P. Yang, Phys. Rev. B **18** (1978), 2304.
- 18) R. J. Baxter, *Exactly Solved Models in Statistical Mechanics* (Academic Press, London, 1982); R. J. Baxter, J. Phys. A **13** (1980), L61; R. J. Baxter and S. K. Tsang, J. Phys. A **13** (1980), 1023; R. J. Baxter and P. A. Pearce, J. Phys. A **15** (1982), 897.
- 19) F. Y. Wu, Rev. Mod. Phys. **54**, (1982), 235.
- 20) A. Chubukov, Phys. Rev. Lett. **69** (1992), 832.
- 21) P. Lecheminant, B. Bernu, C. Lhuillier, L. Pierre, and P. Sindzingre, Phys. Rev. B **56**

- (1997), 2521.
- 22) Ch. Waltdmann, H.-U. Everts, B. Bernu, C. Lhuillier, P. Sindzingre, P. Lecheminant, and L. Pierre, *Eur. Phys. J. B* **2** (1998), 501.
 - 23) K. Hida, *J. Phys. Soc. Jpn.* **70** (2001), 3673.
 - 24) D. C. Cabra, M. D. Grynberg, P. C. W. Holdsworth, and P. Pujol, *Phys. Rev. B* **65** (2002), 094418.
 - 25) D. C. Cabra, M. D. Grynberg, P. C. W. Holdsworth, A. Honecker, P. Pujol, J. Richter, D. Schmalfuß, and J. Schulenburg, *Phys. Rev. B* **71** (2005), 144420.
 - 26) M. E. Zhitomirsky, *Phys. Rev. Lett.* **88** (2002), 057204.
 - 27) S. S. Sosin, L. A. Prozorova, A. I. Smirnov, A. I. Golov, I. B. Berkutov, O. A. Petrenko, G. Balakrishnan, M. E. Zhitomirsky, *Phys. Rev. B* **71** (2005), 094413.
 - 28) O. V. Lounasmaa, *Experimental Principles and Methods Below 1K, chapter 5* (Academic Press, London, 1974).
 - 29) J. A. Barclay and W. A. Steyert, *Cryogenics* **22** (1982), 73.
 - 30) E. F. Shender, *Zh. Éksp. Teor. Fiz.* **83** (1982), 326 [*Sov. Phys. JETP* **56** (1982), 178].